

Theoretical study of contact-mode triboelectric nanogenerators as an effective power source†

Cite this: DOI: 10.1039/c3ee42571a

Simiao Niu,^{‡a} Sihong Wang,^{‡a} Long Lin,^a Ying Liu,^a Yu Sheng Zhou,^a Youfan Hu^a and Zhong Lin Wang^{*ab}

Received 30th July 2013

Accepted 25th September 2013

DOI: 10.1039/c3ee42571a

www.rsc.org/ees

A theoretical model for contact-mode TENGs was constructed in this paper. Based on the theoretical model, its real-time output characteristics and the relationship between the optimum resistance and TENG parameters were derived. The theory presented here is the first in-depth interpretation of the contact-mode TENG, which can serve as important guidance for rational design of the TENG structure in specific applications.

1. Introduction

Scavenging mechanical energy from the ambient environment has attracted worldwide attention. Among all of the available technologies, contact-electrification enabled nanogenerators, *i.e.* triboelectric nanogenerators (TENGs), emerge as a new energy technology with numerous advantages, including large output power, high efficiency, and easy fabrication with low cost. The basic working principle for TENGs is a combination of contact electrification^{1–4} and electrostatic induction. Based on the charge separation mechanism, TENGs can be divided into two categories: contact-mode TENGs based on vertical charge polarization^{5–9} and sliding-mode TENGs based on in-plane charge polarization.^{10–12} The contact-mode TENG has been demonstrated to have numerous applications both as a power source^{5–8} and as an active sensor.⁹ However, there is still a lack of a systematic theoretical model in this field. Experimentally, it is known that the maximum power on a load as provided by the TENG is a result of matching between the TENG and the load.^{6,7} However, a thorough theoretical understanding about how the structural parameters and operation conditions of a TENG

affect the match with the load is still missing, which is critical for designing a compatible TENG for a specific application.

In this paper, a comprehensive theoretical model is built for the contact-mode TENG. Utilizing the derived equation, the real-time output characteristics of the TENG are mathematically modelled. Then based on the calculation results, we clarified the physics behind the three-working-region behaviour and the optimum load resistance. Finally, the quantitative relationship of the optimum resistance with the parameters of the TENG is derived to provide guidance for rational design of TENGs for a specific load.

2. The V – Q – x relationship for contact-mode TENGs

The most important theoretical equation for representing the real-time power generation of a TENG is a relationship among three parameters: the voltage (V) between the two electrodes, the amount of transferred charge (Q) in between, and the separation distance (x) between the two triboelectric charged layers, which can be named the V – Q – x relationship.¹³ Based on the materials for the triboelectric pairs, the contact-mode TENG is mainly divided into two categories: dielectric-to-dielectric and conductor-to-dielectric types. The model built for a dielectric-to-dielectric contact-mode TENG is shown in Fig. 1a. The two dielectric plates, with thicknesses of d_1 and d_2 and the relative dielectric constants ϵ_{r1} and ϵ_{r2} , respectively, are stacked face to face as two triboelectric layers. At the outer surface of these two dielectrics, two metal layers are deposited as two electrodes. The distance (x) between the two triboelectric layers can be varied under the agitation of mechanical force. After being forced to get in contact with each other, the inner surfaces of the two triboelectric layers will have opposite static charges (tribo-charges) with equal density of σ , as a result of contact electrification. For insulators as discussed, it is reasonable to assume that the tribo-charges are uniformly distributed at the two surfaces with negligible decay.^{14,15} When the two triboelectric layers start to separate from each other, with increased x , a potential difference (V) between the two electrodes will be

^aSchool of Material Science and Engineering, Georgia Institute of Technology, Atlanta, Georgia 30332-0245, USA. E-mail: zhwang@gatech.edu

^bSatellite Research Facility, MANA, International Center for Materials Nanoarchitectonics, National Institute for Materials Science, 1-1 Namiki, Tsukuba, 305-0044, Japan

† Electronic supplementary information (ESI) available. See DOI: 10.1039/c3ee42571a

‡ These authors contributed equally to this work.

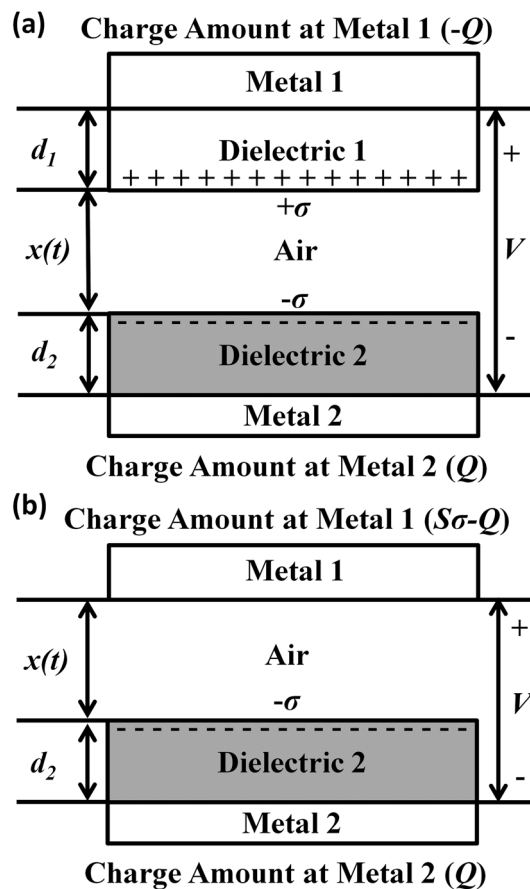


Fig. 1 Theoretical models for (a) dielectric-to-dielectric contact-mode TENG and (b) conductor-to-dielectric contact-mode TENG.

induced. The amount of transferred charges between the two electrodes, as driven by the induced potential, is defined as Q , which also represents the instantaneous amount of charges on each electrode (with opposite signs).

With the above model, the V - Q - x relationship of such a contact-mode TENG can be derived based on electrodynamics. Since the area size (S) of the metals is several orders of magnitude larger than their separation distance ($d_1 + d_2 + x$) in the experimental case, it is reasonable to assume that the two electrodes are infinitely large. Under this assumption, the charges on the metal electrodes will uniformly distribute on the inner surfaces of the two metals. Inside the dielectrics and the air gap, the electric field only has the component in the direction perpendicular to the surface, with the positive value pointing to Metal 2. From the Gauss theorem, the electric field strength at each region is given by

$$\text{Inside Dielectric 1: } E_1 = -\frac{Q}{S\epsilon_0\epsilon_{r1}} \quad (1)$$

$$\text{Inside the air gap: } E_{\text{air}} = -\frac{\frac{Q}{S} + \sigma(t)}{\epsilon_0} \quad (2)$$

$$\text{Inside Dielectric 2: } E_2 = -\frac{Q}{S\epsilon_0\epsilon_{r2}} \quad (3)$$

The voltage between the two electrodes can be given by

$$V = E_1d_1 + E_2d_2 + E_{\text{air}}x \quad (4)$$

Substituting eqn (1)-(3) into eqn (4), we can obtain the V - Q - x relationship for the dielectric-to-dielectric TENG in contact-mode, which is given by

$$V = -\frac{Q}{S\epsilon_0} \left(\frac{d_1}{\epsilon_{r1}} + \frac{d_2}{\epsilon_{r2}} + x(t) \right) + \frac{\sigma x(t)}{\epsilon_0} \quad (5)$$

Similarly, the model for the conductor-to-dielectric category is built, as shown in Fig. 1b. In this structure, we no longer have Dielectric 1 and now Metal 1 plays two roles: both as the top triboelectric layer and as the top electrode. Therefore, the total charges in Metal 1 now have two parts: one is the triboelectric charges ($S\sigma$), the other is the transferred charges between the two electrodes ($-Q$). Thus, the total charges in Metal 1 are ($S\sigma - Q$).

From a similar derivation, the V - Q - x relationship for this model is given by

$$V = E_2d_2 + E_{\text{air}}x = -\frac{Q}{S\epsilon_0} \left(\frac{d_2}{\epsilon_{r2}} + x(t) \right) + \frac{\sigma x(t)}{\epsilon_0} \quad (6)$$

Eqn (6) is exactly the same equation as eqn (5) if $d_1 = 0$. If we define the effective thickness constant d_0 as $d_1/\epsilon_{r1} + d_2/\epsilon_{r2}$ for eqn (5) and d_2/ϵ_{r2} for eqn (6), the V - Q - x relationship for both these two types can be unified as the following equation.

$$V = -\frac{Q}{S\epsilon_0} (d_0 + x(t)) + \frac{\sigma x(t)}{\epsilon_0} \quad (7)$$

3. Output characteristics under different load resistances

Eqn (7) is the basic equation for the contact-mode TENG and can be utilized to calculate its output property. First, two special cases of the open-circuit (OC) condition and short-circuit (SC) condition are analysed. At OC condition, there is no charge transfer, which means that Q is 0. Therefore, the open-circuit voltage V_{OC} is given by

$$V_{\text{OC}} = \frac{\sigma x(t)}{\epsilon_0} \quad (8)$$

At SC condition, V is 0. Therefore, the transferred charges are

$$Q_{\text{SC}} = \frac{S\sigma x(t)}{d_0 + x(t)} \quad (9)$$

$$I_{\text{SC}} = \frac{dQ_{\text{SC}}}{dt} = \frac{S\sigma d_0}{(d_0 + x(t))^2} \frac{dx}{dt} = \frac{S\sigma d_0 v(t)}{(d_0 + x(t))^2} \quad (10)$$

In general cases that a contact-mode TENG is connected to an arbitrary resistor R , the output properties can be estimated by combining eqn (7) with Ohm's law:

$$V = IR = R \frac{dQ}{dt} \quad (11)$$

Merging eqn (11) and eqn (7), we can have

$$R \frac{dQ}{dt} = -\frac{Q}{S\epsilon_0} (d_0 + x(t)) + \frac{\sigma x(t)}{\epsilon_0} \quad (12)$$

This is a first-order ordinary differential equation and can be solved by specifying the boundary condition. Consider the case that at $t = 0$, the two plates are close to each other for a sufficiently long time and then the top plate starts to separate from the bottom one. Therefore, we have the boundary condition of

$$Q(t = 0) = 0 \quad (13)$$

Then eqn (12) can be solved analytically as

$$Q(t) = \sigma S - \sigma S \exp\left[-\frac{1}{RS\epsilon_0} \left(d_0 t + \int_0^t x(t) dt\right)\right] - \frac{\sigma d_0}{R\epsilon_0} \exp\left[-\frac{1}{RS\epsilon_0} \left(d_0 t + \int_0^t x(t) dt\right)\right] \times \int_0^t \exp\left[\frac{1}{RS\epsilon_0} \left(d_0 z + \int_0^z x(z) dz\right)\right] dz. \quad (14)$$

Therefore, the current and voltage output can be derived as

$$I(t) = \frac{dQ}{dt} = -\frac{\sigma d_0}{R\epsilon_0} + \frac{\sigma(d_0 + x(t))}{R\epsilon_0} \exp\left[-\frac{1}{RS\epsilon_0} \left(d_0 t + \int_0^t x(t) dt\right)\right] + \frac{\sigma d_0}{R\epsilon_0} \times \frac{d_0 + x(t)}{RS\epsilon_0} \exp\left[-\frac{1}{RS\epsilon_0} \left(d_0 t + \int_0^t x(t) dt\right)\right] \times \int_0^t \exp\left[\frac{1}{RS\epsilon_0} \left(d_0 z + \int_0^z x(z) dz\right)\right] dz \quad (15)$$

$$V(t) = RI(t) = -\frac{\sigma d_0}{\epsilon_0} + \frac{\sigma(d_0 + x(t))}{\epsilon_0} \exp\left[-\frac{1}{RS\epsilon_0} \left(d_0 t + \int_0^t x(t) dt\right)\right] + \frac{\sigma d_0}{\epsilon_0} \times \frac{d_0 + x(t)}{RS\epsilon_0} \exp\left[-\frac{1}{RS\epsilon_0} \left(d_0 t + \int_0^t x(t) dt\right)\right] \times \int_0^t \exp\left[\frac{1}{RS\epsilon_0} \left(d_0 z + \int_0^z x(z) dz\right)\right] dz. \quad (16)$$

In a special case of uniform motion at a constant velocity (v), the above equations can be further simplified to eqn (17)–(19), as shown below. (The detailed derivation is given in the ESI, Session 1†)

$$Q(t) = \sigma S \left[1 - \exp(-At - Bt^2) + \sqrt{2}F \exp(-At - Bt^2) \times \text{Dawson}\left(\frac{F}{\sqrt{2}}\right) - \sqrt{2}F \times \text{Dawson}\left(\frac{F}{\sqrt{2}} + \sqrt{Bt}\right) \right] \quad (17)$$

$$I(t) = \sigma S \left[\exp(-At - Bt^2)(A + 2Bt) - \sqrt{2}F \times \exp(-At - Bt^2)(A + 2Bt) \times \text{Dawson}\left(\frac{F}{\sqrt{2}}\right) - A + 2A\left(\frac{F}{\sqrt{2}} + \sqrt{Bt}\right) \times \text{Dawson}\left(\frac{F}{\sqrt{2}} + \sqrt{Bt}\right) \right] \quad (18)$$

$$V(t) = \sigma SR \left[\exp(-At - Bt^2)(A + 2Bt) - \sqrt{2}F \times \exp(-At - Bt^2)(A + 2Bt) \times \text{Dawson}\left(\frac{F}{\sqrt{2}}\right) - A + 2A\left(\frac{F}{\sqrt{2}} + \sqrt{Bt}\right) \times \text{Dawson}\left(\frac{F}{\sqrt{2}} + \sqrt{Bt}\right) \right]. \quad (19)$$

The constants A , B , and F are defined by

$$A = \frac{d_0}{RS\epsilon_0} \quad (20.1)$$

$$B = \frac{v}{2RS\epsilon_0} \quad (20.2)$$

$$F = \frac{A}{\sqrt{2B}} = \frac{d_0}{\sqrt{RS\epsilon_0 v}}. \quad (20.3)$$

The Dawson's integral ($\text{Dawson}(x)$) in the above expressions is shown as

$$\text{Dawson}(x) = \exp(-x^2) \int_0^x \exp(y^2) dy. \quad (21)$$

The basic properties of the Dawson's integral are listed in Session 2 of the ESI.†^{16,17}

From the above equations, we notice that the transferred charge, current, and voltage are directly proportional to the tribo-charge surface density (σ). Therefore, σ will only affect the magnitude of Q , I , and V , but not their shape and variation trend with both time and R . σ is mainly affected by the intrinsic material properties of the two triboelectric layers and roughness of the contact surfaces. Thus, through choosing materials at the two ends of the triboelectric series diagram¹⁸ and an appropriate surface fabrication method, σ can be increased and then the performance of the device can be enhanced.

In real experimental cases, the movement of the top plate always has a maximum distance (x_{\max}). As x reaches x_{\max} , the current starts to decay exponentially (ESI, Session 3†). For the uniform motion shown as eqn (22), the numerical calculation results can be obtained by specifying the parameters, which are shown in Table 1.

$$x = vt \left(t < \frac{x_{\max}}{v} \right) \quad (22.1)$$

$$x = x_{\max} \left(t \geq \frac{x_{\max}}{v} \right). \quad (22.2)$$

The real-time output properties for a contact-mode TENG are plotted in Fig. 2 with different load resistances. The detailed profiles of the charge, current, and voltage relationships at

Table 1 Parameters utilized in the constant velocity theoretical calculation

Dielectric 1	Metal, $d_1 = 0 \mu\text{m}$
Dielectric 2	$d_2 = 125 \mu\text{m}$, $\epsilon_{r2} = 3.4$
Area size of the Dielectrics S	58.0644 cm^2 (9 inch ²)
Tribo-charge surface density σ	$10 \mu\text{C m}^{-2}$
Maximum separation distance x_{\max}	0.001 m
Average velocity v	0.1 m s^{-1}

different loads are shown in Fig. 2a–c. At SC condition, the charge transfers at the fastest speed. For a relatively small R , Q can still get its saturation value when the top electrode stops moving ($t = 10$ ms). However, when R is more than 100 M Ω , at $t = 10$ ms, the charge cannot get saturated due to the limit charge transfer rate by the resistor, resulting in the unstopped charge transfer from Metal 1 to Metal 2 after $t = 10$ ms. Therefore, the current is a peak-shape when R is small while the current continues increasing during the plate movement when R is large. The voltage has the same profile with the current, but a different trend in magnitude. The peak values of the voltage, current and power on different loads are displayed in Fig. 2d and e. It can be clearly observed that the operation of the TENG can be divided into three working regions. First, in Region I where the resistance is low (0.1 – 1000 Ω), the peak current has approximately no drop from SC condition, which is due to the similar charge transfer process in comparison with that of SC condition. As a result, the maximum voltage is approximately proportional to the external resistance. Thus, the TENG can be considered as an ideal current source if we only consider the peak value of the output. On the other hand, when the resistor is larger than 1 G Ω (Region III), the output characteristics are close to OC condition, in which the maximum voltage saturates at V_{OC} . In terms of the load property, the TENG works as a constant-voltage source. The medium range of the resistance is Region II, where the maximum current drops dramatically but

the maximum voltage increases at a reverse trend. Around 100 M Ω inside this region, the TENG reaches its maximum instantaneous output power.

These unique output characteristics of TENGs can be interpreted both physically and mathematically. Physically, the working principle of a TENG is a conjunction of the triboelectric process and the electrostatic induction. When the tribo-charges are separated, an induced voltage will be generated between the two electrodes, which will drive the electrons to flow from Electrode 2 to Electrode 1. The electric field from these transferred charges will screen the original electric field from the tribo-charges. The charge accumulation rate at SC condition is the maximum charge transfer rate, which is determined by the moving mode. However, as there is an external load with certain resistance, the resistor will limit the real charge transfer rate, making it lower than that at SC condition. When the load resistance is very small, this limitation is not obvious so that the rate can still catch up with the maximum rate determined by the moving mode, enabling the Q to stay close to Q_{SC} in Region I. When the load resistance continues to increase and gets into Region II, it begins to significantly limit the charge flow rate, making the charge accumulation curve deviate downward from Q_{SC} . As the load resistance is large enough, the transfer of electrons from Metal 2 to Metal 1 is rather slow, which results in a very small current. The induced voltage between the two electrodes will hold for a long time due to the little screening effect, with the magnitude approaching V_{OC} . This is Region III of the TENG.

Mathematically, this can be interpreted from the behaviour of the Dawson's integral. When R is small, the parameters F and B (as defined in eqn (20)) approach infinity. In this region, utilizing the first-order asymptotic series of the Dawson's integral, the following approximate equation can be obtained. (Detailed derivation is shown in the ESI, Session 4.†)

$$I(t) = \frac{\sigma v A}{R \epsilon_0 (A + 2Bt)^2} = \frac{\sigma v d_0 S}{(d_0 + vt)^2}. \quad (23)$$

This is just the same equation as I_{SC} . Therefore, within this region satisfying the first-order asymptotic series (Region I), the behaviour of the charge transfer (*i.e.* the current) remains similar to that of SC condition.

When R is very large, the parameters F and B are close to 0. At this time, the Dawson's integral can be approximated by its first-order Maclaurin series and the following equation can be obtained. (Detailed derivation is shown in the ESI, Session 4.†)

$$V(t) = \frac{\sigma vt}{\epsilon_0}. \quad (24)$$

This is the expression of V_{OC} , so the TENG is now in the quasi-OC condition, which is Region III.

When R is neither too large nor too small, the behaviour of the TENG is in the transitional region between SC and OC conditions (Region II), within which the maximum power is reached, as shown in Fig. 2f.

Besides the uniform motion, the dynamic output properties under other types of motion can be theoretically studied as well.

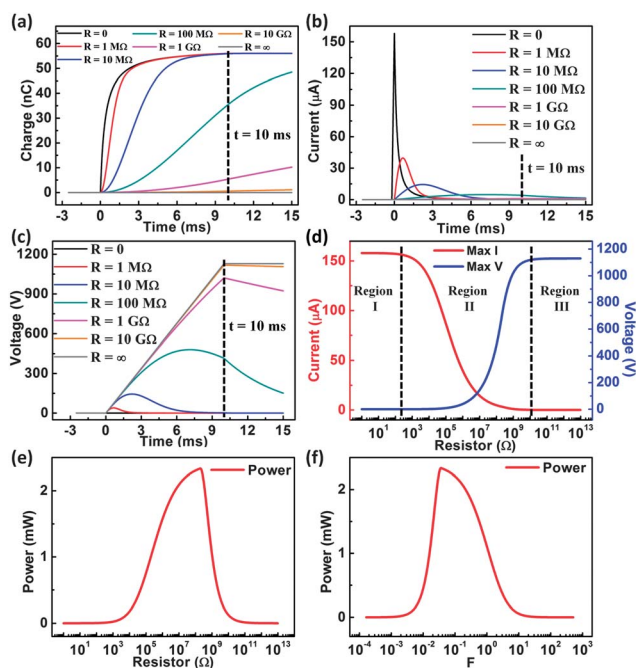


Fig. 2 Calculated output characteristics when the plates are separated at a uniform velocity. The top plate reaches the maximum separation distance and stops moving at $t = 10$ ms. (a) Real-time transferred charge–time relationship at different load resistances. (b) Real-time current–time relationship at different load resistances. (c) Real-time voltage–time relationship at different load resistances. (d) The influence of the load resistance on the magnitude of the output current and voltage. Three working regions are marked. (e) The influence of the load resistance on the instantaneous power output. (f) The influence of the defined F parameter on the instantaneous power output.

We take the cosine moving mode as an example (Fig. 3), which is a lot closer to the realistic case. The $x \sim t$ relationship is shown in eqn (25), in which all the symbols and the parameters are the same as the previous simulation.

$$x = x_{\max} \left[\frac{1}{2} - \frac{1}{2} \cos \left(\frac{\pi v}{x_{\max}} t \right) \right], \quad \left(t < \frac{x_{\max}}{v} \right) \quad (25.1)$$

$$x = x_{\max} \left(t \geq \frac{x_{\max}}{v} \right) \quad (25.2)$$

Numerical calculation results for this moving mode are obtained utilizing eqn (14)–(16) and plotted in Fig. 3. The charge, current and voltage curves are quite similar to the previous results, as shown in Fig. 3a–c. The most obvious difference is that the current peak value does not occur at $t = 0$ due to the process that the top electrode is first accelerated and then decelerated. Thus, because of the screening effect of the transferred charges, its maximum value is much smaller than that from the uniform motion with the same average speed. The dependence of the output properties on the resistance is shown in Fig. 3d–f. Similarly, the TENG also has three working regions. But when R is around 1 M Ω , the current peak value has a slight increase with the resistor. This is because that in this region of resistance, the increase of resistance will promote the limitation of the charge transfer, thus weakening the screen effect, which will possibly elevate the instantaneous

driving force for the current from the unscreened potential difference.

Moreover, in this three-working-region behaviour of the TENG, the optimum resistance for the maximum instantaneous power is a key parameter to maximize the effective efficiency of the TENG. Therefore, the position of the optimum resistance needs to be systematically studied to find its relationship with the TENG's structural parameters and operational conditions, so that the TENG can be rationally controlled for different application purposes.

The optimum resistance can be mathematically investigated under an arbitrary motion for the TENG model built above. We first decompose an arbitrary smooth moving mode with an average velocity v into a series of polynomial moving-mode, which is shown in the equations below.

$$x = \sum_{n=1}^{\infty} \alpha_n \frac{v^n}{x_{\max}^{n-1}} t^n, \quad \left(t < \frac{x_{\max}}{v} \right) \quad (26.1)$$

$$x = x_{\max} \left(t \geq \frac{x_{\max}}{v} \right) \quad (26.2)$$

α_n is the coefficient of n^{th} polynomial moving-mode, and satisfies the following equation.

$$\sum_{n=1}^{\infty} \alpha_n = 1 \quad (26.3)$$

If we substitute this equation into the general equation of the current (eqn (15)), the current under arbitrary moving mode can be given as

$$\begin{aligned} I(t) = & -\frac{\sigma d_0}{R\epsilon_0} + \frac{\sigma d_0}{R\epsilon_0} \left(1 + \sum_{n=1}^{\infty} \frac{\alpha_n v^n}{d_0 x_{\max}^{n-1}} t^n \right) \\ & \times \exp \left[-\frac{1}{RS\epsilon_0} \left(d_0 t + \sum_{n=1}^{\infty} \frac{\alpha_n v^n}{(n+1)x_{\max}^{n-1}} t^{n+1} \right) \right] \\ & + \frac{\sigma d_0}{R\epsilon_0} \times \frac{d_0}{RS\epsilon_0} \left(1 + \sum_{n=1}^{\infty} \frac{\alpha_n v^n}{d_0 x_{\max}^{n-1}} t^n \right) \\ & \times \exp \left[-\frac{1}{RS\epsilon_0} \left(d_0 t + \sum_{n=1}^{\infty} \frac{\alpha_n v^n}{(n+1)x_{\max}^{n-1}} t^{n+1} \right) \right] \\ & \times \int_0^t \exp \left[\frac{1}{RS\epsilon_0} \left(d_0 z + \sum_{n=1}^{\infty} \frac{\alpha_n v^n}{(n+1)x_{\max}^{n-1}} z^{n+1} \right) \right] dz \quad \left(t \leq \frac{x_{\max}}{v} \right) \end{aligned} \quad (27)$$

Since the current starts to decay exponentially when t is larger than x_{\max}/v (ESI Session 3[†]), the peak value of the current can only exist inside the closed interval $[0, x_{\max}/v]$. In order to find the time (t_{\max}) of the current peak, we take the differentiation of $I(t)$ and the time t_0 satisfies the following equation.

$$\left(\frac{dI}{dt} \right)_{t=t_0} = 0 \quad (28)$$

When R is small ($R < 100$ M Ω in Fig. 2), the peak value appears between $t = 0$ and $t = x_{\max}/v$ and t_{\max} is equal to t_0 . When R is large enough ($R > 1$ G Ω in Fig. 2), t_0 is larger than x_{\max}/v , so the current will increase monotonically between

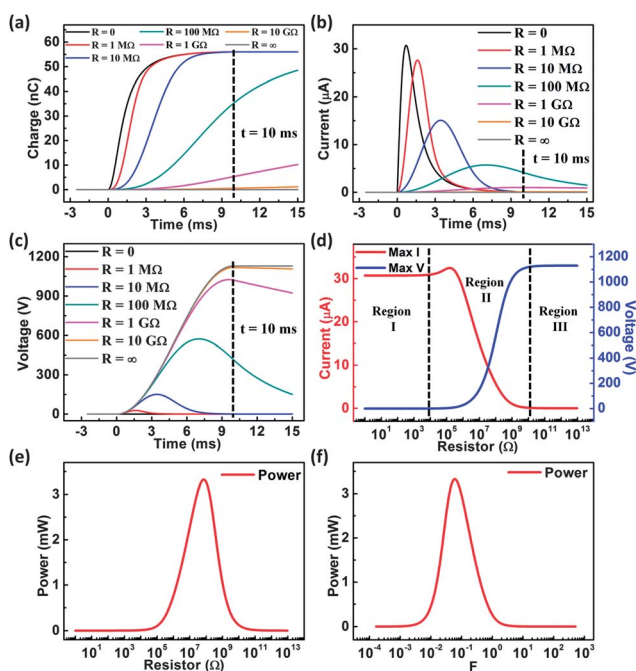


Fig. 3 Calculated output characteristics for a separation distance that is described by a cosine function. The top plate reaches the maximum separation distance and stops moving at $t = 10$ ms. (a) Real-time transferred charge–time relationship at different load resistances. (b) Real-time current–time relationship at different load resistances. (c) Real-time voltage–time relationship at different load resistances. (d) The influence of the load resistance on the magnitude of the output current and voltage. Three working regions are marked. (e) The influence of the load resistance on the instantaneous power output. (f) The influence of the defined F parameter on the instantaneous power output.

$t = 0$ and $t = x_{\max}/v$. Then, t_{\max} is equal to x_{\max}/v . Thus, in the entire region of R , t_{\max} is the minimum value of t_0 and x_{\max}/v , which can be given by

$$t_{\max} = \min\left(t_0, \frac{x_{\max}}{v}\right) \quad (29)$$

With the thickness factor y defined as eqn (30), t_0 can be proven to be a function (f) of F and y , (detailed derivation is shown in the ESI, Session 5†) as shown in eqn (31):

$$y = \frac{x_{\max}}{d_0} \quad (30)$$

$$t_0 = \frac{x_{\max}}{v} f(F, y) \quad (31)$$

Therefore, we have

$$t_{\max} = \min\left(t_0, \frac{x_{\max}}{v}\right) = \frac{x_{\max}}{v} \min(f(F, y), 1) = \frac{x_{\max}}{v} M(F, y) \quad (32)$$

where M is another function. Substituting eqn (32) into eqn (27), the peak value of the current I_{\max} can be given by (detailed derivation is shown in the ESI, Session 5†)

$$I_{\max} = \frac{\sigma d_0}{R \epsilon_0} G(F, y) \quad (33)$$

where G is a new function. Then, the peak instantaneous power is

$$P_{\max} = I_{\max}^2 R = \frac{(\sigma d_0)^2}{\epsilon_0^2} \times \frac{1}{R} G^2(F, y) = \frac{\sigma^2 S v}{\epsilon_0} F^2 G^2(F, y) \quad (34)$$

The optimum load resistance R_{opt} satisfies the following equation:

$$\frac{\partial P_{\max}}{\partial R} = 0 \quad (35)$$

Therefore, combining eqn (34) and eqn (35), the optimum resistance satisfies the following equation: (detailed derivation is shown in the ESI Session 5†)

$$G(F_{\text{opt}}, y) + F_{\text{opt}} \left(\frac{\partial G}{\partial F} \right)_{F=F_{\text{opt}}} = 0 \quad (36)$$

Eqn (36) shows that the optimum value of F is only a function of y . Therefore,

$$F_{\text{opt}} = H(y) = \frac{d_0}{\sqrt{R_{\text{opt}} S \epsilon_0 v}} \quad (37)$$

where the function H only relies on the moving mode.

Thus, the expression of R_{opt} can be given by

$$R_{\text{opt}} = \frac{d_0^2}{F_{\text{opt}}^2 S v \epsilon_0} = \frac{d_0^2}{[H(y)]^2 S v \epsilon_0} = \frac{d_0^2}{\left[H\left(\frac{x_{\max}}{d_0}\right) \right]^2 S v \epsilon_0} \quad (38)$$

More specifically, if the TENG is operated in uniform motion and the thickness ratio of x_{\max} and d_0 (y) is larger than 10 (which is usually the case in the experiment to obtain an effective charge transfer), the $H(y)$ function in eqn (38) can be approximately solved, as shown below. (Detailed derivation is shown in the ESI, Session 6.†)

$$F_{\text{opt}} = H(y) \approx \frac{1}{1+y} \quad (39)$$

Now the optimum resistance can be approximately given by

$$R_{\text{opt}} = \frac{d_0^2}{F_{\text{opt}}^2 S v \epsilon_0} \approx \frac{(d_0 + x_{\max})^2}{S v \epsilon_0} \quad (40)$$

This equation can be utilized to estimate the optimum resistance for a TENG. Although for different moving modes, the actual optimum resistance will somewhat deviate from this estimated value, it can serve as a good reference when a TENG is designed for driving a specified load with certain resistance, so that the actual power on the load can be maximized. Then we can use the precise expression of eqn (38) together with the experimental measurement to further optimize the geometry parameters.

To verify the above relationship, numerical calculations were carried out under uniform motion with different parameters, as shown in Fig. 4. Without special notation in the figure, the values utilized for the parameters are exactly the same as those in Table 1. As shown in Fig. 4a and b, R_{opt} is inversely proportional to either the area size (S) or the average velocity (v) while F_{opt} is not dependent on neither of these two parameters. These numerical calculated results are consistent with eqn (38). On the other hand, the influence of effective dielectric thickness and air gap distance on R_{opt} and F_{opt} is displayed in Fig. 4c and d. If we keep the ratio (y) of the above two thicknesses (d_0 and x_{\max}) to be 27.2, R_{opt} is proportional to d_0^2 while F_{opt} remains the same. However, if only one of the effective dielectric thickness or the gap distance is changed so that the ratio (y) varies, F_{opt} will not remain constant, as shown in Fig. S2.† R_{opt} increases with either the effective dielectric thickness or the gap distance.

To further validate the theoretical equation presented above, a set of experiments was designed and carried out to compare

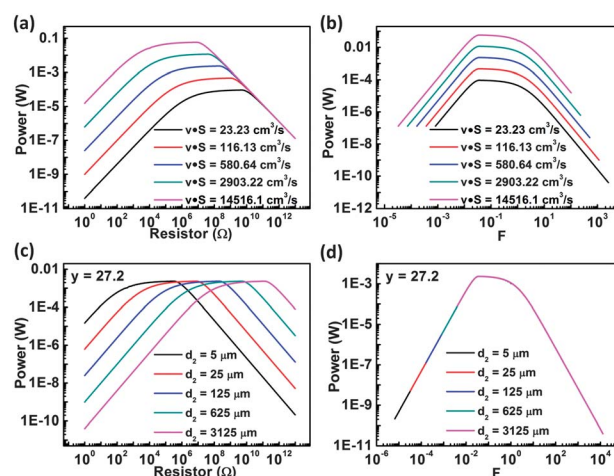


Fig. 4 Influence of the TENG's parameters on the optimum resistance under uniform velocity of separation. (a and b) Maximum output power profile with (a) load resistance and (b) different products of velocity and area size. (c and d) Maximum output power profile with (c) load resistance and (d) F under different effective dielectric thicknesses and gap distances with maintaining their ratio to be 27.2.

with the theoretical expectations. The fabricated TENG is structurally the same as that shown in Fig. 1b. The triboelectric pairs were chosen as Al and Kapton films. The metal electrode was deposited on one side of the Kapton film. Two Acrylic sheets were used as supporting substrates. The bottom plate is bonded on the measurement platform and the top plate is driven by a linear motor that has a cosine motion. In the first set of experiments, the same device was measured under different average velocities, as shown in Fig. 5a. When the average velocities are 0.02 m s^{-1} , 0.04 m s^{-1} , and 0.08 m s^{-1} , the derived optimum load resistance (through interpolation of the experiment data) is $14.2 \text{ M}\Omega$, $6.66 \text{ M}\Omega$, and $4.08 \text{ M}\Omega$, respectively, which shows the same trend as the theoretical estimation. In the other set of measurements, the influence of the gap and the dielectric thickness is experimentally studied, as shown in Fig. 5b. The thickness of the Kapton film (d_k) in device 1 is $25 \mu\text{m}$ while that of device 2 is $125 \mu\text{m}$, and the corresponding gaps (x_{max}) are 2 mm and 10 mm , respectively, which maintain the same y . Through the measurement on a series of resistors with all the other parameters kept the same, the obtained optimum resistance for device 1 is $7.69 \text{ M}\Omega$ while that of device 2 is $162.3 \text{ M}\Omega$. The experimental optimum resistance ratio is 21.1 , which is quite close to 25 , as the theoretical estimation value. All of the above experimental results further validate the conclusions

from the theoretical derivation above, showing its potential to guide the real experimental designs.

Besides the mathematical analysis, we can address the relationship of the optimum resistance trend and the change of the parameters from the underlying physical process. As discussed above, the optimum resistance is reached in the middle of Region II, and thus will probably shift with the shift trend of Region II, in which the maximum charge transfer rate I_{SC} determined by the motion of the plate is relatively close to the real charge transfer rate. The real charge transfer rate is V/R , with the maximum possible value as V_{OC}/R . An increase in the area size of the TENG will contribute to elevating I_{SC} while having no effect on V_{OC} . Therefore, in order to keep V_{OC}/R in the same range, a lower resistance is needed to balance this influence of device size. Therefore, Region II shifts to the lower resistance range, which will reduce the optimum resistance. Similarly, increasing the average velocity boosts I_{SC} while maintaining the same value for V_{OC} . As a result, the optimum resistance will decrease. If the effective dielectric thickness increases, I_{SC} decreases while V_{OC} keeps the same value. Thus, the optimum resistance increases. In addition, increasing the gap will reduce I_{SC} while increase V_{OC} , which will increase the optimum resistance. From similar analysis, since the change in the tribo-charge density will increase I_{SC} and V_{OC} at the same ratio, the optimum resistance will not be affected.

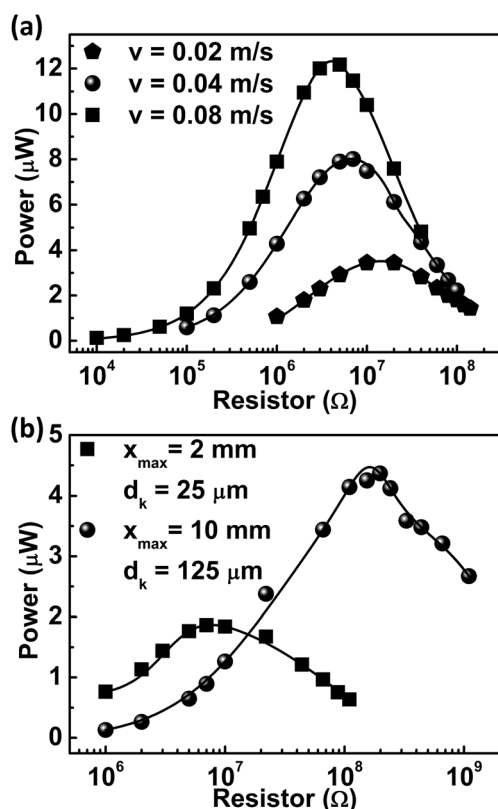


Fig. 5 Measured optimum resistance under different TENG parameters. The dots are measured values and the lines are obtained through interpolation of the experimental data. (a) Maximum output power profile with load resistance at different average velocities. (b) Maximum output power profile with load resistance at different Kapton film thicknesses and gap distances with their ratio remaining constant.

4. Conclusions

In summary, a theoretical model for contact-mode TENGs is presented in this work. The analytical model was built for both dielectric-to-dielectric and conductor-to-dielectric contact-mode TENGs and their basic equations (V - Q - x relationship) were derived. From the basic equation, the real-time output characteristics were presented, showing three-working-region behaviour when driving external resistance loads. The reason for this unique characteristic was mathematically interpreted. We further systematically studied the optimum resistance for the maximum instantaneous power and the influence of the TENG parameters, such as area size, average velocity, effective dielectric thickness, and the gap distance. Additionally, experiments were performed to verify these theoretical expected results. The theory presented here is the first in-depth interpretation and analysis of the contact-mode TENG's working principle, clearly showing its unique operation characteristics, which will be able to serve as important guidance for rational design of the device structure as a power source in specific applications and self-powered systems.

Acknowledgements

This research was supported by the U.S. Department of Energy, the Office of Basic Energy Sciences (Award DE-FG02-07ER46394), NSF (0946418), MANA, and the World Premier International Research Center Initiative (WPI Initiative), MEXT, Japan, through a laboratory at the Georgia Institute of Technology.

Notes and references

- 1 R. G. Horn, D. T. Smith and A. Grabbe, *Nature*, 1993, **366**, 442–443.
- 2 R. G. Horn and D. T. Smith, *Science*, 1992, **256**, 362–364.
- 3 L. S. McCarty and G. M. Whitesides, *Angew. Chem., Int. Ed.*, 2008, **47**, 2188–2207.
- 4 H. T. Baytekin, A. Z. Patashinski, M. Branicki, B. Baytekin, S. Soh and B. A. Grzybowski, *Science*, 2011, **333**, 308–312.
- 5 F. R. Fan, Z. Q. Tian and Z. L. Wang, *Nano Energy*, 2012, **1**, 328–334.
- 6 G. Zhu, C. F. Pan, W. X. Guo, C. Y. Chen, Y. S. Zhou, R. M. Yu and Z. L. Wang, *Nano Lett.*, 2012, **12**, 4960–4965.
- 7 S. H. Wang, L. Lin and Z. L. Wang, *Nano Lett.*, 2012, **12**, 6339–6346.
- 8 X. S. Zhang, M. D. Han, R. X. Wang, F. Y. Zhu, Z. H. Li, W. Wang and H. X. Zhang, *Nano Lett.*, 2013, **13**, 1168–1172.
- 9 L. Lin, Y. N. Xie, S. H. Wang, W. Z. Wu, S. M. Niu, X. N. Wen and Z. L. Wang, *ACS Nano*, 2013, **7**, 8266–8274.
- 10 S. H. Wang, L. Lin, Y. N. Xie, Q. S. Jing, S. M. Niu and Z. L. Wang, *Nano Lett.*, 2013, **13**, 2226–2233.
- 11 L. Lin, S. H. Wang, Y. N. Xie, Q. S. Jing, S. M. Niu, Y. F. Hu and Z. L. Wang, *Nano Lett.*, 2013, **13**, 2916–2923.
- 12 G. Zhu, J. Chen, Y. Liu, P. Bai, Y. S. Zhou, Q. S. Jing, C. F. Pan and Z. L. Wang, *Nano Lett.*, 2013, **13**, 2282–2289.
- 13 S. M. Niu, Y. Liu, S. H. Wang, L. Lin, Y. S. Zhou, Y. F. Hu and Z. L. Wang, *Adv. Mater.*, DOI: 10.1002/adma.201302808.
- 14 L. H. Lee, *J. Electrostat.*, 1994, **32**, 1–29.
- 15 F. Saurenbach, D. Wollmann, B. D. Terris and A. F. Diaz, *Langmuir*, 1992, **8**, 1199–1203.
- 16 J. H. McCabe, *Math. Comput.*, 1974, **28**, 811–816.
- 17 N. J. A. Sloane, *Lect. Notes Artif. Int.*, 2007, **4573**, 130.
- 18 A. F. Diaz and R. M. Felix-Navarro, *J. Electrostat.*, 2004, **62**, 277–290.